Rheologica Acta (2023) 62:461–472
https://doi.org/10.1007/s00397-023-01409-9

ORIGINAL CONTRIBUTION

Bidisperse magnetorheological fluids utilizing composite polypyrrole nanotubes/magnetite nanoparticles and carbonyl iron microspheres

Andrei Munteanu[1] · Tomáš Plachý[1] · Lenka Munteanu[1] · Fahanwi Asabuwa Ngwabebhoh[1] · Jaroslav Stejskal[1] · Miroslava Trchová[2] · Michal Kubík[3] · Michal Sedlačík[1,4]

Received: 16 May 2023 / Revised: 14 July 2023 / Accepted: 15 July 2023 / Published online: 2 August 2023

Abstract

Conductive polypyrrole nanotubes were synthesized with a two-step one-pot synthesis. During synthesis, the nanotubes were decorated with magnetite nanoparticles at different concentrations granting them magnetic properties. The characterization of the tubes revealed differences from the theoretical reactions. A bidisperse magnetorheological fluid (MRF) was prepared by mixing the composite polypyrrole nanotubes/magnetite nanoparticles with commercial carbonyl iron spherical microparticles in silicone oil. The rheological properties of the bidisperse system were studied under the presence of magnetic field at room and elevated temperature. An enhancement of the MR effect with the presence of the nanotubes was observed when compared with a standard MRF consisted only of magnetic microparticles. Due to the faster magnetic saturation of the nanotubes, this enhancement is exceptionally high at low magnetic fields. The stability of the system is studied under dynamic conditions where it is revealed that the nanotubes keep the standard particles well dispersed with the sedimentation improving by more than 50%.

Keywords Magnetic composite · Polypyrrole nanotubes · Magnetorheology · Bidisperse system · Sedimentation Stability

Introduction

A magnetorheological fluid (MRF) is a unique type of smart material which may alter its viscosity by several orders of magnitude within milliseconds upon exposure to an external magnetic field (de Vicente et al. 2011). A typical MRF is composed of micrometre-sized magnetic particles suspended in a non-magnetic carrier liquid. Due to its ability to change from liquid to solid-like state, several applications are involved. Brakes, clutches, and shock absorbers are the most common examples (Bai et al. 2019; Zainordin et al. 2021; Park et al. 2021; Deng et al. 2021).

Despite the plethora of studies and applications, these MRFs still face prominent problems such as corrosion at high temperatures and aggressive environments, coagulation due to the unfavourable interactions between the particles and liquid carrier, and lastly sedimentation caused by the density mismatch of the components. Several solutions have been proposed to overcome these problems, most notably using various additives, different morphologies, and coating the magnetic particles (Stejskal et al. 2021a; Thiagarajan and Koh 2021). Another approach would be the addition of rod-like particles in the suspension (Sedlacik and Pavlinek 2017), thus creating a bidisperse system (or also called dimorphic, a system in which the dispersed phase particles are of two different morphologies or size). Such dimorphic magnetorheological fluids (DMRFs) decrease the sedimentation effect to acceptable levels and prevent the coagulation due to the steric repulsions provided by the rod-like particles (Sedlacik et al. 2013). The majority of bidisperse studies however are focused on the interactions between spheres with heavily mismatched size. These studies have shown that sedimentation stability is significantly increased (Wang et al.

✉ Michal Sedlačík
msedlacik@utb.cz

1 Centre of Polymer Systems, University Institute, Tomas Bata University in Zlín, 760 01 Zlín, Czech Republic

2 University of Chemistry and Technology Prague, 6, 166 28 Prague, Czech Republic

3 Faculty of Mechanical Engineering, Institute of Machine and Industrial Design, Brno University of Technology, 616 69 Brno, Czech Republic

4 Department of Production Engineering, Faculty of Technology, Tomas Bata University in Zlín, 760 01 Zlín, Czech Republic

2021b). Nonetheless, inconsistencies are observed in regard to the volume fraction of smaller particles. At lower fractions, the small particles fill the gaps in the chain-like structures formed by the bigger ones when an external magnetic field is applied; however; higher concentrations could cause an inferior performance (Wereley et al. 2006; Chand et al. 2014). Other types of bidisperse systems include the addition of rod-like particle into a conventional MRF composed of micron spheres. Current studies include different types of rods, mainly divided to magnetic and non-magnetic ones. Apart from improving the viability of such MRFs, these rod-like particles may also improve the mechanical properties, such as higher yield stress when an external magnetic field is applied (on-state). Jiang et al. (2011) successfully synthesized a DMRF using magnetic Fe nanowires, showing both a major reduction in sedimentation and better rheological properties which were observed even at low magnetic fields. Unfortunately, these nanowires are prone to oxidation and have relatively high values of coercivity and remanent magnetization. This could lead to a short life span of the system. Ngatu et al. (2008) also used similar nanowires with a higher length resulting in improved stability, but the rheological properties remained roughly the same. Eventually, oxidation was resolved using coated particles; however, the magnetic properties of these samples were severely hindered (Sedlacik et al. 2013). Non-magnetic rods also may show improvements in mechanical properties, leading to the conclusion that these improvements are caused mainly by the shape of the particles. This was further validated by Bombard et al. (2014), who investigated the stoichiometric ratio of the two components, illustrating that these systems are more efficient at low rod concentrations.

With the basic concepts already investigated, the way is paved for more complex DMRFs. A novel DMRF using polypyrrole (PPy) nanotubes decorated with magnetite, Fe_2O_3, which may alter their magnetic properties based on their preparation, is presented. It is important to note that this is one of the first reports of a DMRF composed of magnetic spheres and nanotubes. In a preliminary work, the effect of the tube morphology and the magnetic and conducting properties of these nanotubes was studied (Stejskal et al. 2021b). Polypyrrole nanotubes were chosen for several reasons. First, the synthesis of such tubes is proven to be quick and facile. As mentioned above, some MRFs are prone to oxidation; however, PPy nanotubes have shown antioxidant activity (Upadhyay and Kumar 2013). Moreover, non-magnetic PPy nanotubes are very versatile being able to find a utilization in several applications including actuation, batteries, conductive inks, electromagnetic interference shielding, sensors, and electrorheological fluids (Stejskal and Trchová 2018). In addition, non-magnetic PPy nanotubes have been used in medical applications including adsorbing influenza viruses, antimicrobial activity, necrolysis, and tissue engineering (Liao et al. 2014; Ivanova et al. 2017). Magnetic nanorods have been already used in biomedical applications (Nikolaou et al. 2021), thus further increasing the interest of magnetic PPy nanotubes. For the majority of literature, the rod/tube-like particles are notable smaller than the spherical one. Wang et al. (2021a) studied a DMRF with both tubes and spherical particles being in the range of ~10 nm with great results. Lastly, several DMRFs were prepared using creative materials and morphologies with the majority focusing on the sedimentation stability; however, their MR performance was inferior (Wang et al. 2018; Cvek et al. 2018; Marins et al. 2019).

In this work, composite magnetic PPy nanotubes were synthesized using a novel method, and subsequently, their magnetic properties were studied together with other physical properties. Following, several bidisperse systems were prepared, and their (magneto)rheological properties were studied and compared with a standard MRF. Lastly, the thermal stability of the DMRF is evaluated together with the sedimentation stability in a dynamic environment as a closer comparison to the actual applications.

Materials and methods

Synthesis of the magnetic nanotubes

Polypyrrole nanotubes were synthesised and decorated with magnetite nanoparticles during a two-step synthesis. Two samples were synthesised at different molarities of iron(III) chloride hexahydrate ($FeCl_3{\cdot}6H_2O$) (>99%) which was provided by Sigma-Aldrich together with the rest of the chemicals that are mentioned in this part. Table 1 presents the amount of each component used with the mole ratio of $FeCl_3{\cdot}6H_2O$ over pyrrole represented as n. For the synthesis, firstly, the pyrrole (>97%) was dispersed in water (0.2 M in 100 mL), with methyl orange (0.004 M in 100 mL) being added later on. The dye is the key substance which guides the growth of tube-like morphology instead of spheres (Mori et al. 2017). Aside, the second solution of $FeCl_3{\cdot}6H_2O$ in water ($FeCl_3{\cdot}6H_2O$ is 0.5 M in 100 mL for n=2.5 and 1.2 M in 100 mL for n=6) was prepared. Right after, both solutions were combined, and the polymerization of pyrrole to the PPy nanotubes was completed at room temperature once

Table 1 Preparation compositions for PPy/magnetite nanotubes

	N	Pyrrole (mL)	$FeCl_3{\cdot}6H_2O$ (g)	Water (mL)	Methyl orange (mg)
Sample 1	2.5	1.4	13.52	200	130
Sample 2	6	1.4	32.45	200	130

the mixture turned dark brown/black and thickened with the procedure taking a few minutes.

Figure 1 shows the main synthesis reactions. The final molar concentrations of the reaction mixture are 0.1-M pyrrole and 0.25-M $FeCl_3 \cdot 6H_2O$ for n=2.5 and 0.6 M for n=6 and 0.002-M methyl orange. To decorate the PPy nanotubes with magnetite, the resulting PPy dispersion was mixed with an excessive amount of ammonium hydroxide (4 M) at room temperature until the solution became basic (pH > 10). The pH was periodically confirmed using a pH meter. Lastly, the decorated nanotubes were isolated by filtration and washed with ethanol. The particles were left to dry overnight at 60 °C.

The final yields were 5.4 g for n=2.5 and 10.6 g for n=6. The abovementioned reactions are described in detail in a previous work, focusing only on the synthesis of the rods and perfecting the molar ratios, during which it was possible to tune the conductivity and the magnetic properties of the nanotubes by changing the molar ratio n (Stejskal et al. 2021b). However, to obtain magnetic nanoparticles with higher magnetization saturation, the deprotonation with ammonium hydroxide was modified using ammonium hydroxide with a much higher concentration in this work. For n=2.5, all $FeCl_3 \cdot 6H_2O$ should be consumed by the reaction (Fig. 1) to produce the PPy nanotubes in the base form. For n=6, the excess amount converts the mixture of $FeCl_3$ and $FeCl_2$ to magnetite and decorate the nanotubes.

Characterization of particles

The ATR FTIR spectra of the powdered samples were obtained using the Nicolet 6700 spectrometer (Thermo-Nicolet, USA) equipped with a reflective ATR extension GladiATR (PIKE Technologies, USA) and a diamond crystal. The spectra were recorded in the 4000–400-cm^{-1} range with a DLaTGS (deuterated L-alanine doped triglycine sulphate) detector at resolution of 4 cm^{-1}, 64 scans, and a Happ-Genzel apodization. The morphology of PPy particles decorated with magnetite was studied by scanning electron microscope NOVA NanoSEM 450 (FEI, the Netherlands), while their magnetic saturation was investigated using a vibrating sample magnetometer (VSM, Model 7407, USA) with the intensity of magnetic field in a range from −10 to +10 kOe.

The specific surface area of the samples was estimated using nitrogen adsorption/desorption measurement using a surface area analyser (BELSORP-mini II, BEL Japan, Inc., Japan). The data was treated with a Brunauer, Emmett, and Teller (BET) multipoint method. Thermogravimetric analysis (TGA; TGA Q500, TA Instruments, New Castle, USA) was performed in air in temperature range 25–700 °C using a heating rate 10 °C min^{-1}.

Preparation of the dimorphic magnetorheological fluids

For the dimorphic system, carbonyl iron (CI) spherical particles (CN grade, iron content >99.5%, d_{50}=6.5–8.0 µm; BASF, Germany) were mixed with the magnetic composite PPy nanotubes/magnetite nanoparticles in silicone oil (Lukosiol M200, Chemical Works Kolín, Czech Republic; viscosity 194 mPa s, density 0.965 g cm^{-3}) at various concentrations. Before preparation, the particles (both PPy nanotubes and iron microspheres) were dried overnight at high vacuum at 80 °C along with the oil to remove possible moisture. Several DMRFs were prepared with the code-names and compositions shown in Table 2.

The newly prepared DMRFs were always measured with the following techniques immediately after their preparation. Meanwhile, a sonication process was applied using an ultrasonic bath to ensure that no aggregates were formed.

Characterization of the dimorphic magnetorheological fluids

The rotational rheometer Physica MCR 502 (Anton Paar, Graz, Austria) was employed to investigate the flow

Table 2 Composition of the prepared magnetorheological fluids in vol%

Components	Code name		
	MRF 2.5	MRF 6	Standard MRF
Carbonyl iron	10	10	10
PPy/Fe_3O_4 nanotubes (n=2.5)	1	0	0
PPy/Fe_3O_4 nanotubes (n=6)	0	1	0
Silicone oil	89	89	90

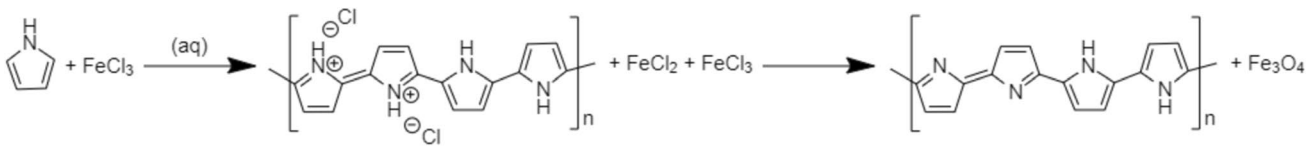

Fig. 1 The two-step synthesis of magnetic nanotubes; PPy nanotubes are first created using the oxidation of the pyrrole with $FeCl_3 \cdot 6H_2O$. Excess amounts of $FeCl_3 \cdot 6H_2O$ led to the creation of magnetite under alkaline conditions converting PPy to a base form

properties of the MRFs. To determine the effect of the magnetic field, a magneto-cell (Physica MRD 180/1T) was employed. The samples were exposed to various external magnetic fields up to 1050 kA m^{-1}. A temperature control was achieved using an additional external bath. All samples were measured using a parallel-plate geometry of 20 mm with rough surface. The gap was set at 1 mm for all measurements since this parameter is proved to affect the rheological properties (Jonkkari et al. 2012). Before each test, the samples were stirred at shear rate $(\dot{\gamma})$ of 50 s^{-1} for a minute to redisperse them. The measurements were performed in the shear rate range of 0.01 to 200 s^{-1} to ensure no overflow happens during the measurements. Flow curves were performed in the abovementioned range steadily increasing the magnetic field starting with 150 kA m^{-1} and increasing it by intervals of 300 kA m^{-1}. After the final flow curve at 1050 kA m^{-1}, the sample was redispersed and a second flow curve was performed with the magnetic field off to evaluate the impact of previews on-state measurements. Step-wise increases of magnetic field were performed under steady shear of 50 s^{-1} during which the magnetic field was turned on and off every 20 s, each time increasing by 150 kA m^{-1}. The same tests were repeated at 60 °C. The dynamic sedimentation tests were performed in the following way. The samples were pre-sheared at 50 s^{-1} for a minute to redisperse the particles. Then, the shear rate was removed with a low magnetic field of 300 A m^{-1} applied. The field was then removed and shear of 10 s^{-1} was reapplied. The sedimentation was calculated as the ratio of the current shear stress over the shear stress captured right after the field was removed thus at the start of the off-state.

Results and discussion

Characterization of the polypyrrole/magnetite particles

FTIR spectroscopy

To confirm the successful synthesis of the targeted tubes, their ATR FTIR spectra are compared with the spectra of related and well-established particles, as presented in Fig. 2. The infrared spectrum of the "standard" PPy nanotubes (PPyNT) exhibits the main bands with maxima at 1514 cm^{-1} (C–C-stretching vibrations in the pyrrole ring), at 1435 cm^{-1} (C–N-stretching vibrations in the ring), at 1283 cm^{-1} (C–H or C–N in-plane deformation modes), at 1128 and 1088 cm^{-1} (breathing vibrations of the pyrrole rings), and at 998 cm^{-1} (C–H and N–H in-plane deformation vibrations). In addition, the peaks located at 955 and 832 cm^{-1} correspond to the C–H out-of-plane deformation

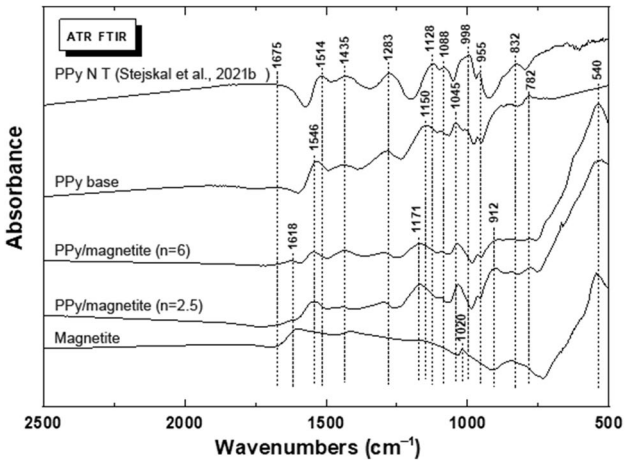

Fig. 2 The ATR FTIR spectra of the magnetic composite PPy nanotubes/magnetite nanoparticles compared with the spectra of "standard" PPy nanotubes, PPy base, and magnetite (Stejskal et al. 2016, 2021b, a; Stejskal and Trchová 2018)

vibrations of the ring (Stejskal and Trchová 2018; Stejskal et al. 2021a). The infrared spectra of the PPy nanotubes are recorded in Fig. 2. The PPy/magnetite n=6 and 2.5 exhibit a peak at 1618 cm^{-1}, a maximum at 1546 cm^{-1}, and further notable peaks at 1435, 1283, and 1171 cm^{-1}, and also at 1088, 1045, and 912 cm^{-1}. The shifts of the main bands can be observed when compared to the spectrum of the "standard" PPy base, this corresponds to a slight deprotonation of the samples which was discussed in detail in a previous work (Stejskal et al. 2016, 2021b). The deprotonation is also reflected in the intensity decrease of the broad band observed above 1800 cm^{-1}. The presence of magnetite is detected in the spectra by the peaks observed in its spectrum and by the enhancement of the intensity of the broad absorption band below 900 cm^{-1}.

Morphology

The particles' morphology of both composites based on differing molarities was studied by SEM, as presented in Fig. 3.

As can be seen, the nanotubular morphology of PPy was confirmed with a nano-scaled diameter and a length in micrometre range. Furthermore, the PPy/magnetite (n=6) particles (Fig. 3b) exhibit obvious magnetite coating (the presence of magnetite was also confirmed via FTIR and VSM). However, the n=2.5 counterpart also shows the magnetite presence (Fig. 3a), albeit in a lower amount. This hints that a residual amount of $FeCl_3 \cdot 6H_2O$ was indeed present after the reaction, even though for n=2.5, theoretically, all $FeCl_3$ oxidant should have been consumed and no magnetite thus produced, as mentioned in the synthesis section.

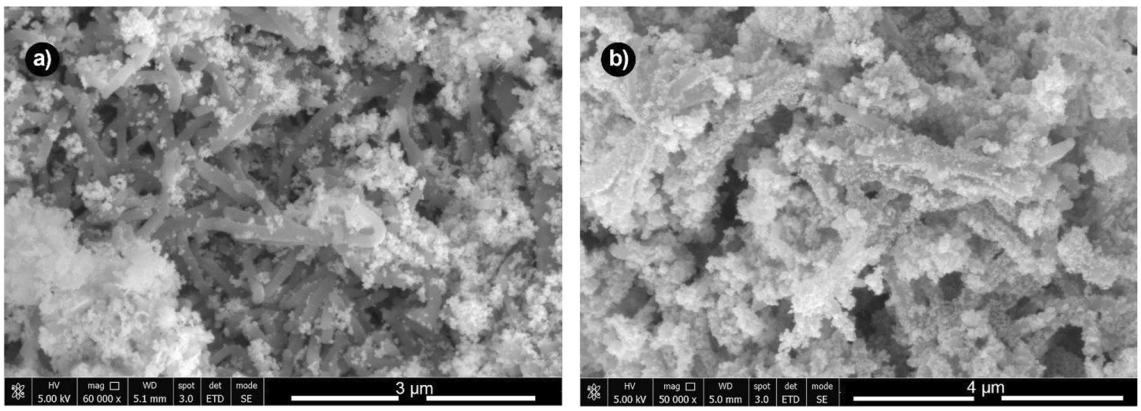

Fig. 3 Scanning electron microscopy of PPy/magnetite particles based on different molarities of $FeCl_3 \cdot 6H_2O$: n=2.5 (**a**) and n=6 (**b**)

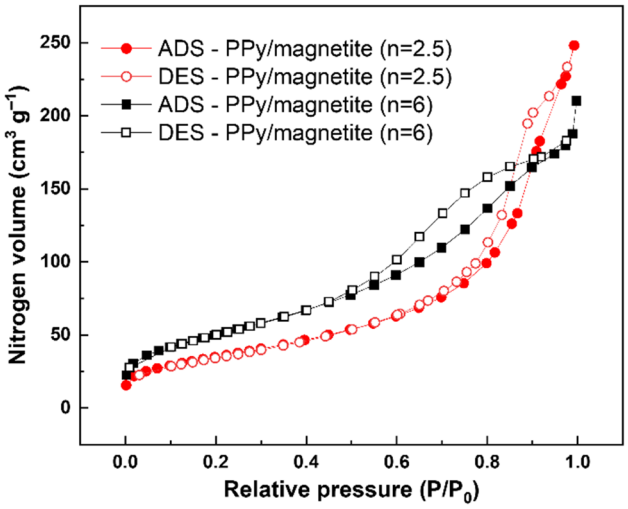

Fig. 4 Nitrogen adsorption and desorption isotherms of the prepared composite particles: PPy/magnetite (n=2.5) and PPy/magnetite (n=6)

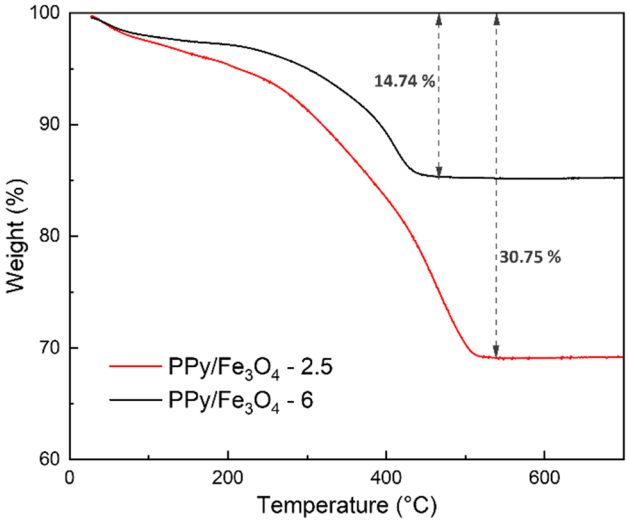

Fig. 5 Thermogravimetric analysis of prepared composite particles PPy/Fe_3O_4. Experiments were performed in an air atmosphere using heating rate 10 °C min^{-1}

Surface properties

The different mole ratio of the precursors used during the synthesis also affected the surface area of the prepared composite particles (Fig. 4). While PPy/magnetite (n=2.5) particles exhibited specific surface area 126 m^2 g^{-1}, the sample PPy/magnetite (n=6) possessed higher surface area 183 m^2 g^{-1} due to the presence of nanosized magnetite particles. Furthermore, the shape of adsorption and desorption curves indicated solid surface of the particles with the presence of micropores.

Thermogravimetric analysis

Thermogravimetric analysis of the composite PPy/magnetite particles in air (Fig. 5) showed that the sample PPy/magnetite (n=6) exhibited significantly lower drop in weight (~15%) than the second sample (~30%). While iron oxide particles during TGA treatment commonly exhibit only insignificant drop in weight (Jafari-Soghieh et al. 2019), PPy in air can be fully decomposed (Plachy et al. 2013). The mass loss should be then ascribed to PPy decomposition and is more prominent for the sample prepared at n=2.5. The residues represent the magnetite particles, and as can be clearly seen, their higher content can be found in the sample PPy/magnetite (n=6) as expected.

Magnetic properties

The composite PPy/magnetite particles exhibited magnetic properties, as illustrated in Fig. 6. The composites prepared at n=2.5 and n=6 were analysed. The synthesised particles

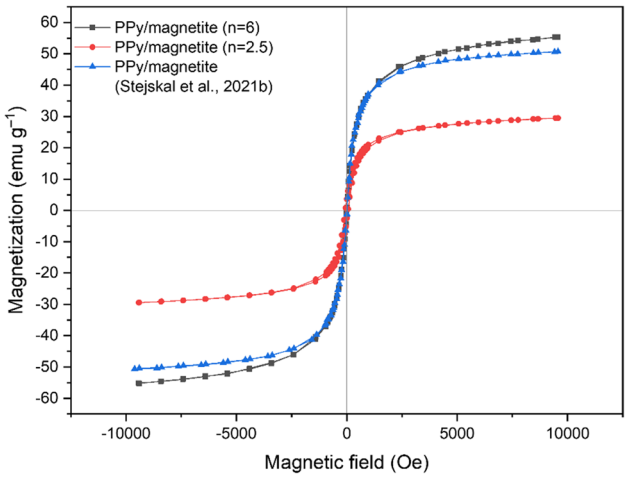

Fig. 6 Magnetic properties PPy/magnetite nanotubes composite prepared at different molarities and compared with their previous alternative as reported in Stejskal et al. (2021b)

were further compared with their analogue from a previously published report (Stejskal et al. 2021b) for a reference.

As can be seen, the newly synthesised PPy/magnetite peaked at 55.2 emu g^{-1} exceeding the maximum peak of its previous alternative, peaking at 51 emu g^{-1}; thus, this modified synthesis proved to be better. As for the reference comparison, synthesised pure magnetite nanoparticles were reported in the literature with saturation magnetization 65 emu g^{-1} and 62 emu g^{-1} (Qiu et al. 2006; Fekry et al. 2022).

Magnetorheology

The rheological properties of the bidisperse system composed of the magnetic composite PPy nanotubes/magnetite nanoparticles and standard CI microspheres were investigated. The flow curves at various magnetic fields for the MRF 6 are shown in Fig. 7.

The impact of the magnetic field is apparent on the flow curves with the shear stress increasing several orders of magnitude especially at the lower shear rates. With the presence of the magnetic field, the particles are arranged into chain-like structures which significantly increase the shear stress. As the magnetic field is further increased, the rate of stress increase is lower as the magnetization of the particles reaches their saturation values, a typical behaviour of a magnetorheological fluid. For the majority of the experimental window, the shear stress values show a plateau. Apart from the plateau values, the magnetic field also affects its length. To be specific, as can be seen in Fig. 7b, 150 kA m^{-1} is apparent that the hydrodynamic forces are starting to take over the magnetic ones at ~1 s^{-1} with the termination of the plateau and the increase of stress. The critical shear rate can be observed closer to 20 s^{-1}. At saturated fields, i.e. 1050 kA m^{-1}, the data indicates that the chain-like structures become more robust and harder for the hydrodynamic forces to break. Consequently, the magnetic forces dominate over the hydrodynamic ones throughout the majority of the experimental window of the applied shear rate starting from the very low shear rates with such long plateaus being observed before for bidispersed MRFs (Cvek et al. 2022). The dimorphic sample in particular has their plateau length increased when compared with the standard MRF which can be found in supplementary information. Such plateaus can be associated with flow instabilities such as the shear banding phenomenon. Indeed, throughout the entire experimental window and for all measurements where a magnetic field was used, there is shear banding as a result of the chain-like structures that the magnetic particles form essentially phase separating from the liquid carrier. Other shear banding phenomena in colloids and specifically for rod-like particles should not be present as the magnetic interactions between

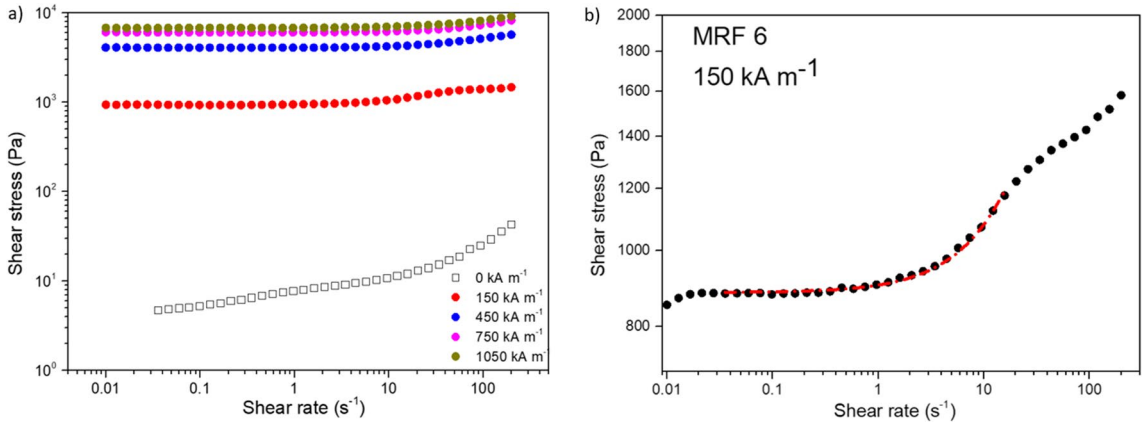

Fig. 7 Flow curves for sample MRF 6 **a** for different magnetic fields and **b** for 150 kA m^{-1}. The red line represents a fit based on the Bingham plastic model

the particles are too strong (Ovarlez et al. 2009; Parisi et al. 2022). This is the case even at high shear rates where the hydrodynamic forces dominate (Martínez-Cano et al. 2023).

The critical shear rate, where the hydrodynamic forces overcome the magnetic ones, is represented by an inclination of the flow curve to the Newtonian behaviour (Stejskal and Trchová 2018). For applications, it is important to keep the magnetic forces dominating for as high shear rates as possible (Wang and Gordaninejad 2006); thus, the present suspension can be characterized as excellent. The rest of the samples share a similar behaviour as shown in the supporting information.

From Fig. 7b, a simple Bingham plastic model was used to extract the yield stress which is shown in Table 3 together with the rest of the samples.

The dimorphic samples show more than two times higher yield stress and lower magnetic fields with the difference being reduced towards the saturated fields. The MRF 6 shows a slightly higher yield stresses although the difference with MRF 2.5 is minor. The increase of the yield stress is explained through the nanotubes which fill the gaps in the chain-like structures formed by the spheres, thus assembling a more robust arrangement (Ashtiani et al. 2015).

Previously, it was mentioned that the magnetic forces dominate over the hydrodynamic ones at lower shear rates. As the shear rate increases, eventually the hydrodynamic forces become relevant. A relevantly good quantity to compare the two types of forces is the Mason number (Mn) which is defined as the ratio between the hydrodynamic forces over the magnetic ones. The well-established behaviour in the study of Klingenberg et al. (2007) was used to calculate the Mn which essentially scales linearly with shear rate and inverse square to the magnetic field $Mn \sim \dot{\gamma} H^{-2}$. The viscosity then was plotted against Mn as can be seen in Fig. 8. For all samples, the Mn is way below unity indicating that the magnetic forces dominate for the entire experimental window. The standard MRF is following the predicted behaviour with the data from different magnetic fields collapsing together. For the dimorphic samples (n=6) however, that is not the case. The curves are not collapsing and tend to move towards lower Mn as the magnetic field is increased indicating stronger magnetic interactions. It is important to note that the Mn calculation includes many assumptions, such as perfect spheres of the same size and simplified magnetic interactions between both types of particles and the particles with the carrier. Regardless, the curves are relevantly close to each other. The same behaviour is observed for MRF 2.5 which can be found in supplementary information (Figure S3). Such discrepancies have been observed before. Literature suggests that at saturated fields, the non-linear magnetization has a significant effect (Klingenberg et al. 2007); however, in our case, the standard MRF is not impacted. Such a discrepancy was also observed in a bidisperse MRF, yet the standard equivalent follows the expected dependency (Cvek et al. 2022). The explanation suggested that the interparticle friction which was not accounted in the theory plays a notable role. Note that we used the same equations to extract the Mn examples mentioned above. Another potential explanation with the Mn not scaling as $Mn \sim \dot{\gamma} H^{-2}$ for DMRFs could be associated with the structure of the chains. The nanotubes are expected to fill the

Table 3 Yield stress in Pa at various magnetic fields for the standard and dimorphic MRFs

Magnetic field (kA m^{-1})	MRF 2.5	MRF 6	Standard MRF
150	895	884	313
450	3974	4216	1801
750	6174	6352	3252
1050	6976	7213	4309

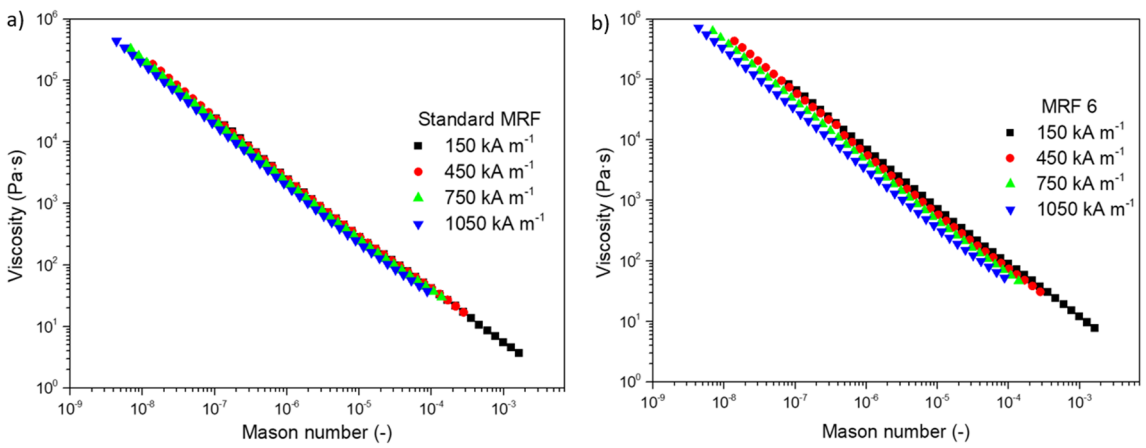

Fig. 8 Viscosity as a function of the Mason number at different magnetic fields and samples: **a** standard MRF and **b** MRF 6

gaps formed during the chain formation of the spheres rather than forming chain-like structures themselves, something that the current theory does not account for (López-López et al. 2005). This phenomenon makes the structures more robust which is reflected in Fig. 8b, as a decrease of Mn or increase of magnetic forces. To conclude, it is obvious that the Mn only describes well spherical systems of relevantly low polydispersity. Magnetorheological fluid studies with unique morphologies and components avoid to present measurements with Mn which should be presented to better understand the overall interactions.

As mentioned above, when a magnetic field is applied, magnetic particles form chain-like structures which cause a vast increase in the shear stress. To evaluate this increase, the stress ratio between the on- and the off-states is studied for different shear rates. The ratio (MR efficiency) is evaluated for all samples at two different magnetic fields, and the results are presented in Fig. 9.

The sample prepared using the PPy nanotubes/magnetite with higher content of magnetite (n=6) shows the highest shear stress increase, higher than the standard MRF with CI only, especially at lower shear rates. The MRF 2.5, on the other hand, displays the lowest stress increase especially in Fig. 9b. It is important to note that MRF 2.5 shows higher shear stress values in comparison with the standard MRF during the on-state as shown in Figure S1. However, the shear stress values during the off-state are also significantly higher due to the presence of rods in the system which keeps the spheres well dispersed and has a reflection in the shear stress values. Notably, at higher shear rates, the differences are less impactful for all samples. At lower magnetic fields, the addition of magnetic composite PPy/magnetite to the standard MRF plays a more pronounced role on the MR performance of the system.

The MR efficiency for the MRF 6 is 3.35 times higher than the standard MRF at 150 kA m^{-1} while only 1.95 times higher at 1050 kA m^{-1}. For the MRF 2.5 on the other hand, the ratio is 1.43 times lower than the standard MRF at 150 kA m^{-1}; however, at 1050 kA m^{-1}, the standard MRF is 3.65 times higher. This behaviour is attributed to the saturation magnetization of the magnetic composite PPy/magnetite which is achieved at lower fields when compared to the CI microspheres (Esmaeilzare et al. 2018), thus saturating "faster". A similar behaviour can be extracted from the yield stress values of Table 3. Thus, the nanotubes share stronger interactions at lower fields forming more robust chain-like structures. The same behaviour was observed for a different dimorphic study where rod-like particles similarly magnetically saturate at lower magnetic fields (Plachy et al. 2017). It can be concluded that the addition of magnetic composite PPy nanotubes/magnetite nanoparticles prepared using the mole ratio oxidant/pyrrole n=6 improved the MR efficiency especially at lower magnetic fields. In real applications, the MRFs are operating at elevated temperatures (McKee et al. 2018; Kumar Kariganaur et al. 2022a). Elevated temperatures may negatively affect the automobile's performance (Ramos et al. 2005; Pavlov 2017). Thus, it is important to evaluate the effect of the temperature on the MR properties of MRFs.

Temperature effect

Figure 10 shows a step-wise increase of magnetic field under steady shear for two different temperatures. During this process, the magnetic field is turned on and off while steadily increasing every 20 s. The sample was then redispersed and the test was repeated at an elevated temperature. For Fig. 10, the values for the 60 °C are shifted by 20 s for clarity.

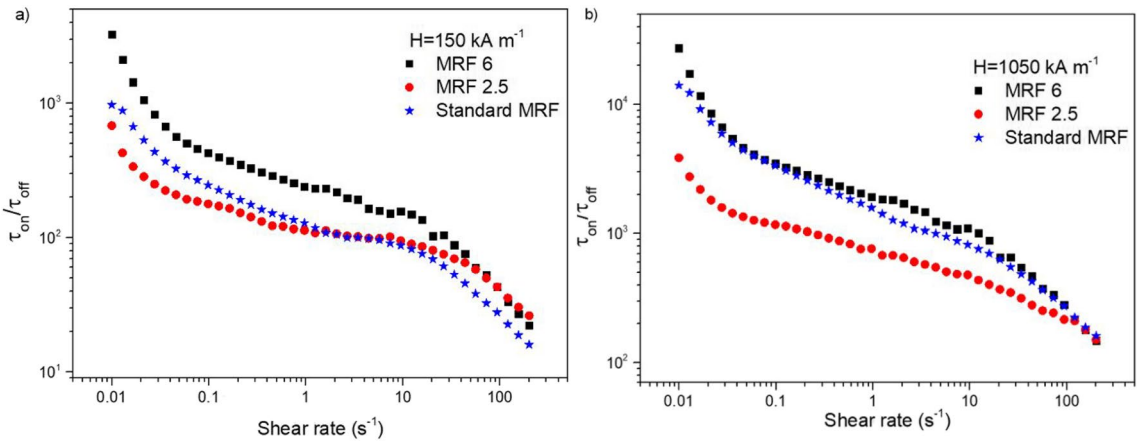

Fig. 9 Magneto-induced shear stress ratio as a function of shear rate for different samples and various magnetic fields: **a** 150 kA m^{-1} and **b** 1050 kA m^{-1}

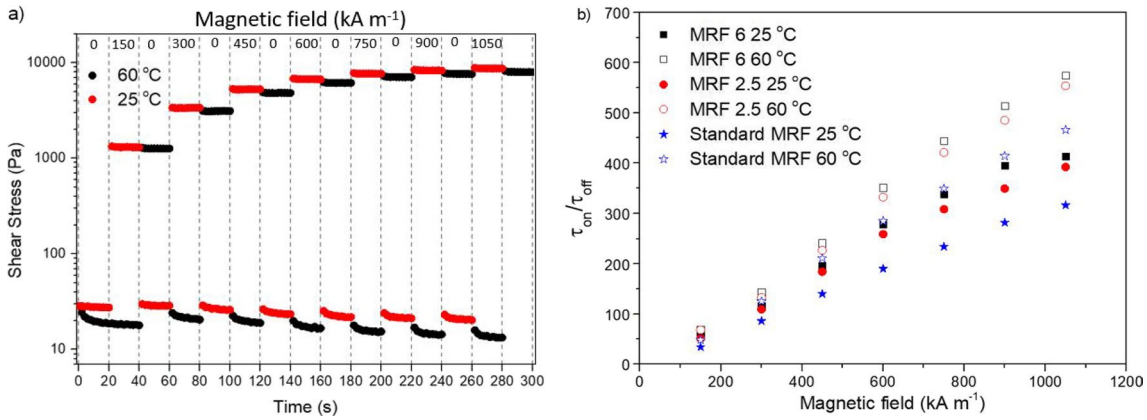

Fig. 10 **a** The effect of step-wise increase of the magnetic field on shear stress under a steady shear of 50 s^{-1} at different temperatures for the sample MRF 6. The changes of the magnetic field are illustrated with dotted lines with the values noted on top. The sample at 25 °C is shifted by 20 s for clarity reasons. **b** Shear stress ratio during the on- and off-state at different magnetic fields for different MRFs at two different temperatures

As can be seen, upon activating the magnetic field, the stress increased instantaneously. In addition, at 60 °C, despite the off-state stress being lower due to the shrinkage of the viscosity of the silicone oil, when the magnetic field is on, the stress values remain nearly the same. It can be concluded that in this case, the chain's strength has little dependence on the viscosity of the carrier as both chain-like structures are almost equally robust. An average shear stress value for the different magnetic fields was extracted, and the MR efficiency between the on- and off-state was then calculated. The results are plotted as a function of the magnetic field together with the rest of the samples (see supporting information) as shown in Fig. 10b.

Both bidisperse systems show a significant increase of their ratio for both temperatures in comparison with the standard MRF especially at higher magnetic fields. This can be explained by the interactions between the PPy nanotubes and CI microspheres. It is known that such bidisperse systems are arranged differently during the off-state (Adams et al. 1998). When a magnetic field is applied, it seems like the particles form the chain-like structures differently due to these interactions leading to a greater MR efficiency. Generally, the MR performances was improved for all samples at 60 °C. This is attributed to the lower shear stress values (thus viscosity) during the off-state while during the on-state, the viscosity values are preserved. Furthermore, several standard MRFs have been investigated at elevated temperatures of the same range with the MR performance showing a similar behaviour (Rabbani et al. 2015; McKee et al. 2018; Li et al. 2021).

Sedimentation assessment

Sedimentation stability is the biggest obstacle to overcome for MRFs as the magnetic particles form permanent aggregates reducing the MR properties of the MRFs. The sedimentation stability of the DMRFs and the standard MRF was studied under constant shear rate of 10 s^{-1} at 60 °C to simulate potential applications. The sedimentation was calculated as the stress of a given time over initial off-state stress. Figure 11 demonstrates the sedimentation stability over time. The sedimentation stability for the bidisperse samples is noticeably enhanced. Despite the elevated temperature which is proven to escalate sedimentation (Kumar Karigan-aur et al. 2022b, a), the dimorphic samples can be compared with other MRFs with increased stability (Sedlacik et al.

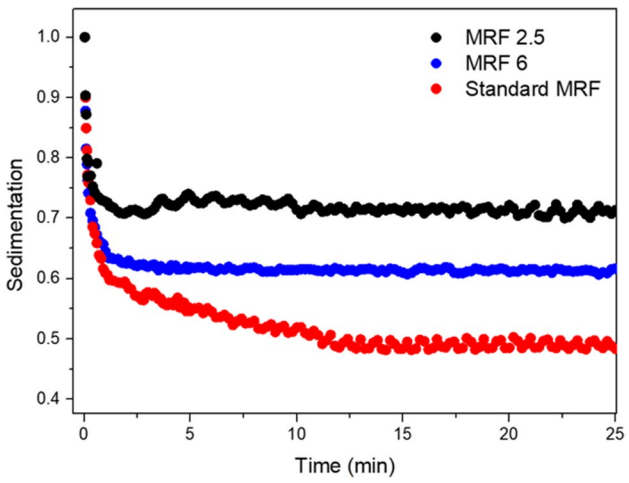

Fig. 11 Dynamic sedimentation tests for various MRFs at shear rate of 10 s^{-1} and 60 °C

2013). Additionally, the standard MRF reached steady state long after the DMRF. In the beginning, it seems like the spheres rapidly sediment; however, this increases the effective particle concentration, and as a result, the sedimentation process is slowed by the interactions of the spheres. The MRF 2.5 shows the best stability, which is attributed to the shape of the rods. As discussed in the particle morphology, the lower amount of magnetite resulted in a higher aspect ratio for the MRF 2.5. Thus, the rods in that specific sample should have stronger entropic repulsions which increases the overall stability. However, it can be assumed that there is sedimentation under shear which may affect the flow curves, especially for the lower shear rates (Russel 1980). The sedimentation of colloidal suspensions has been previously studied rheologically using different techniques showing similar results (Bazilevskii et al. 2010; Ovarlez et al. 2012). The same group showed that when fibres are added, there is a reduction of the sedimentation process similar to our case (Bazilevsky et al. 2017). From the latter, it can be concluded that the sedimentation obstacle must be addressed even during dynamic conditions for certain MRFs.

Conclusions

Two types of magnetic PPy nanotubes decorated with different amount of magnetite were synthesized using a novel method. The magnetic properties of these nanotubes are the highest among their kind and saturate faster than the standard CI spherical particles. A dimorphic magnetorheological suspension using microspheres and nanotubes was prepared. The overall flow behaviour of the dimorphic systems is similar to a standard MRF; however, the DMRFs showed higher magneto-induced shear stress increase. Through this study, it is revealed that faster saturating particles may significantly enhance the MRF's behaviour at lower fields. The samples were also tested at elevated temperatures closer to real applications. The nanotubular morphology helped the system to increase its MR effect. In addition, the stability of the fluids was studied dynamically. Despite the constant rotation of the geometry, the particles continued to settle. The addition of the nanotubes severely increased the viability of the MRFs by more than 50%. To conclude, the magnetic composite PPy nanotubes/magnetite nanoparticles improved both the rheological properties of the corresponding standard MRFs at room and elevated temperatures and their sedimentation stability.

Supplementary Information The online version contains supplementary material available at https://doi.org/10.1007/s00397-023-01409-9.

Funding Open access publishing supported by the National Technical Library in Prague. The authors A.M. and L.M. wish to thank the Internal Grant Agency of Tomas Bata University in Zlín (project no. IGA/CPS/2022/004) for its financial support. The authors A.M. and M.S. gratefully acknowledge project DKRVO (RP/CPS/2022/007), and author T.P. acknowledges project DKRVO (RP/CPS/2022/003) supported by the Ministry of Education, Youth and Sports of the Czech Republic.

Data availability Additionally, most raw data are provided in the SI.

Declarations

Competing interests The authors declare no competing interests.

References

Adams M, Dogic Z, Keller SL, Fraden S (1998) Entropically driven microphase transitions in mixtures of colloidal rods and spheres. Nature 393:349–352. https://doi.org/10.1038/30700

Ashtiani M, Hashemabadi SH, Ghaffari A (2015) A review on the magnetorheological fluid preparation and stabilization. J Magn Magn Mater 374:716–730. https://doi.org/10.1016/j.jmmm.2014.09.020

Bai X-X, Shen S, Wereley NM, Wang D-H (2019) Controllability of magnetorheological shock absorber: I. Insights, modeling and simulation. Smart Mater Struct 28:015022. https://doi.org/10.1088/1361-665X/aaf072

Bazilevskii AV, Koroteev DA, Rozhkov AN, Skobeleva AA (2010) Sedimentation of particles in shear flows of viscoelastic fluids. Fluid Dyn 45:626–637. https://doi.org/10.1134/S0015462810040125

Bazilevsky AV, Kalinichenko VA, Plyashkevich VA et al (2017) Sedimentation of particles in shear flows of viscoelastic fluids with fibers. Rheol Acta 56:787–799. https://doi.org/10.1007/s00397-017-1036-x

Bombard AJF, Gonçalves FR, Morillas JR, de Vicente J (2014) Magnetorheology of dimorphic magnetorheological fluids based on nanofibers. Smart Mater Struct 23:125013. https://doi.org/10.1088/0964-1726/23/12/125013

Chand M, Shankar A, Ali N et al (2014) An improved properties of bidispersed magneto-rheological fluids. RSC Adv. https://doi.org/10.1039/C4RA07431A

Cvek M, Jamatia T, Suly P et al (2022) Stable magnetorheological fluids containing bidisperse fillers with compact/mesoporous silica coatings. Int J Mol Sci 23:11044. https://doi.org/10.3390/ijms231911044

Cvek M, Mrlik M, Moucka R, Sedlacik M (2018) A systematical study of the overall influence of carbon allotrope additives on performance, stability and redispersibility of magnetorheological fluids. Colloids Surf A Physicochem Eng Asp 543:83–92. https://doi.org/10.1016/j.colsurfa.2018.01.046

Deng H, Gao Y, Hu R et al (2021) Self-sensing automotive magnetorheological dampers for low frequency vibration. Smart Mater Struct 30:115015. https://doi.org/10.1088/1361-665X/ac2c5f

de Vicente J, Klingenberg DJ, Hidalgo-Alvarez R (2011) Magnetorheological fluids: a review. Soft Matter 7:3701. https://doi.org/10.1039/c0sm01221a

Esmaeilzare A, Rezaei SM, Ramezanzadeh B (2018) Corrosion and magnetic properties of encapsulated carbonyl iron particles in aqueous suspension by inorganic thin films for magnetorheological finishing application. Appl Surf Sci 436:1200–1212. https://doi.org/10.1016/j.apsusc.2017.12.135

Fekry M, Elmesallamy SM, El-Rahman NRA et al (2022) Eco-friendly adsorbents based on abietic acid, boswellic acid, and chitosan/magnetite for removing waste oil from the surface of the water. Environ Sci Pollut Res 29:64633–64646. https://doi.org/10.1007/s11356-022-20169-2

Ivanova VT, Garina EO, Burtseva EI et al (2017) Conducting polymers as sorbents of influenza viruses. Chem Papers 71:495–503. https://doi.org/10.1007/s11696-016-0068-5

Jafari-Soghieh F, Maleki B, Behniafar H (2019) Effect of dendrimer-functionalized magnetic iron oxide nanoparticles on improving thermal and mechanical properties of DGEBA/IPD epoxy networks. High Perform Polym 31:24–31. https://doi.org/10.1177/0954008317749020

Jiang W, Zhang Y, Xuan S et al (2011) Dimorphic magnetorheological fluid with improved rheological properties. J Magn Magn Mater 323:3246–3250. https://doi.org/10.1016/j.jmmm.2011.07.024

Jonkkari I, Kostamo E, Kostamo J et al (2012) Effect of the plate surface characteristics and gap height on yield stresses of a magnetorheological fluid. Smart Mater Struct 21:075030. https://doi.org/10.1088/0964-1726/21/7/075030

Klingenberg DJ, Ulicny JC, Golden MA (2007) Mason numbers for magnetorheology. J Rheol (N Y N Y) 51:883–893. https://doi.org/10.1122/1.2764089

Kumar Kariganaur A, Kumar H, Arun M (2022a) Effect of temperature on sedimentation stability and flow characteristics of magnetorheological fluids with damper as the performance analyser. J Magn Magn Mater 555:169342. https://doi.org/10.1016/j.jmmm.2022.169342

Kumar Kariganaur A, Kumar H, Arun M (2022b) Influence of temperature on magnetorheological fluid properties and damping performance. Smart Mater Struct 31:055018. https://doi.org/10.1088/1361-665X/ac6346

Liao J, Ning C, Tan G et al (2014) Conducting polypyrrole nanotube arrays as an implant surface: fabricated on biomedical titanium with fine-tunability by means of template-free electrochemical polymerization. Chempluschem 79:524–530. https://doi.org/10.1002/cplu.201300385

Li H, Jönkkäri I, Sarlin E, Chen F (2021) Temperature effects and temperature-dependent constitutive model of magnetorheological fluids. Rheol Acta 60:719–728. https://doi.org/10.1007/s00397-021-01302-3

López-López MT, de Vicente J, Bossis G et al (2005) Preparation of stable magnetorheological fluids based on extremely bimodal iron–magnetite suspensions. J Mater Res 20:874–881. https://doi.org/10.1557/JMR.2005.0108

Marins JA, Plachý T, Kuzhir P (2019) Iron–sepiolite magnetorheological fluids with improved performances. J Rheol (N Y N Y) 63:125–139. https://doi.org/10.1122/1.5048051

Martínez-Cano Ó, Morillas JR, Cvek M et al (2023) High-speed videomicroscopy of sheared carbonyl iron suspensions. Smart Mater Struct 32:025004. https://doi.org/10.1088/1361-665X/acaadc

McKee M, Gordaninejad F, Wang X (2018) Effects of temperature on performance of compressible magnetorheological fluid suspension systems. J Intell Mater Syst Struct 29:41–51. https://doi.org/10.1177/1045389X17705203

Mori DI, Martin RM, Noble RD, Gin DL (2017) Cross-linked, polyurethane-based, ammonium poly(ionic liquid)/ionic liquid composite films for organic vapor suppression and ion conduction. Polymer (Guildf) 112:435–446. https://doi.org/10.1016/j.polymer.2017.01.064

Ngatu GT, Wereley NM, Karli JO, Bell RC (2008) Dimorphic magnetorheological fluids: exploiting partial substitution of microspheres by nanowires. Smart Mater Struct 17:045022. https://doi.org/10.1088/0964-1726/17/4/045022

Nikolaou M, Avraam K, Kolokithas-Ntoukas A et al (2021) Superparamagnetic electrospun microrods for magnetically-guided pulmonary drug delivery with magnetic heating. Mater Sci Eng: C 126:112117. https://doi.org/10.1016/j.msec.2021.112117

Ovarlez G, Bertrand F, Coussot P, Chateau X (2012) Shear-induced sedimentation in yield stress fluids. J Nonnewton Fluid Mech 177–178:19–28. https://doi.org/10.1016/j.jnnfm.2012.03.013

Ovarlez G, Rodts S, Chateau X, Coussot P (2009) Phenomenology and physical origin of shear localization and shear banding in complex fluids. Rheologica Acta, pp 831–844. https://doi.org/10.1007/s00397-008-0344-6

Parisi D, Vlassopoulos D, Kriegs H et al (2022) Underlying mechanism of shear-banding in soft glasses of charged colloidal rods with orientational domains. J Rheol (N Y N Y) 66:365–373. https://doi.org/10.1122/8.0000400

Park J-Y, Kim G-W, Oh J-S, Kim Y-C (2021) Hybrid multi-plate magnetorheological clutch featuring two operating modes: fluid coupling and mechanical friction. J Intell Mater Syst Struct 32:1537–1549. https://doi.org/10.1177/1045389X20988086

Pavlov N (2017) Influence of shock absorber temperature on vehicle ride comfort and road holding. MATEC Web Conf 133:02006. https://doi.org/10.1051/matecconf/201713302006

Plachy T, Cvek M, Kozakova Z et al (2017) The enhanced MR performance of dimorphic MR suspensions containing either magnetic rods or their non-magnetic analogs. Smart Mater Struct 26:025026. https://doi.org/10.1088/1361-665X/aa56ef

Plachy T, Sedlacik M, Pavlinek V et al (2013) An effect of carbonization on the electrorheology of poly(p-phenylenediamine). Carbon N Y 63:187–195. https://doi.org/10.1016/j.carbon.2013.06.070

Qiu G, Wang Q, Nie M (2006) Polypyrrole-Fe_3O_4 magnetic nanocomposite prepared by ultrasonic irradiation. Macromol Mater Eng 291:68–74. https://doi.org/10.1002/mame.200500285

Rabbani Y, Ashtiani M, Hashemabadi SH (2015) An experimental study on the effects of temperature and magnetic field strength on the magnetorheological fluid stability and MR effect. Soft Matter 11:4453–4460. https://doi.org/10.1039/C5SM00625B

Ramos JC, Rivas A, Biera J et al (2005) Development of a thermal model for automotive twin-tube shock absorbers. Appl Therm Eng 25:1836–1853. https://doi.org/10.1016/j.applthermaleng.2004.11.005

Russel WB (1980) Review of the role of colloidal forces in the rheology of suspensions. J Rheol (N Y N Y) 24:287–317. https://doi.org/10.1122/1.549564

Sedlacik M, Pavlinek V (2017) Magnetorheology of dimorphic magnetorheological fluids based on iron nanorods. J Phys Conf Ser 790:012031. https://doi.org/10.1088/1742-6596/790/1/012031

Sedlacik M, Pavlinek V, Vyroubal R et al (2013) A dimorphic magnetorheological fluid with improved oxidation and chemical stability under oscillatory shear. Smart Mater Struct 22:035011. https://doi.org/10.1088/0964-1726/22/3/035011

Stejskal J, Sapurina I, Vilčáková J et al (2021b) Conducting and magnetic composites polypyrrole nanotubes/magnetite nanoparticles: application in magnetorheology. ACS Appl Nano Mater 4:2247–2256. https://doi.org/10.1021/acsanm.1c00063

Stejskal J, Sapurina I, Vilčáková J et al (2021a) One-pot preparation of conducting melamine/polypyrrole/magnetite ferrosponge. ACS

Appl Polym Mater 3:1107–1115. https://doi.org/10.1021/acsapm.0c01331

Stejskal J, Trchová M (2018) Conducting polypyrrole nanotubes: a review. Chem Papers 72:1563–1595. https://doi.org/10.1007/s11696-018-0394-x

Stejskal J, Trchová M, Bober P et al (2016) Polypyrrole salts and bases: superior conductivity of nanotubes and their stability towards the loss of conductivity by deprotonation. RSC Adv 6:88382–88391. https://doi.org/10.1039/C6RA19461C

Thiagarajan S, Koh AS (2021) Performance and stability of magnetorheological fluids—a detailed review of the state of the art. Adv Eng Mater 23:2001458. https://doi.org/10.1002/adem.202001458

Upadhyay J, Kumar A (2013) Engineering polypyrrole nanotubes by 100MeV Si9+ ion beam irradiation: enhancement of antioxidant activity. Mater Sci Eng: C 33:4900–4904. https://doi.org/10.1016/j.msec.2013.08.009

Wang F, Ma Y, Zhang H et al (2021a) Rheological properties and sedimentation stability of magnetorheological fluid based on multi-walled carbon nanotubes/cobalt ferrite nanocomposites. J Mol Liq 324:115103. https://doi.org/10.1016/j.molliq.2020.115103

Wang G, Geng J, Qi X et al (2021b) Rheological performances and enhanced sedimentation stability of mesoporous Fe_3O_4 nanospheres in magnetorheological fluid. J Mol Liq 336:116389. https://doi.org/10.1016/j.molliq.2021.116389

Wang G, Ma Y, Cui G et al (2018) Two-dimensional Fe_3O_4/MoS_2 nanocomposites for a magnetorheological fluid with enhanced sedimentation stability. Soft Matter 14:1917–1924. https://doi.org/10.1039/C7SM02425H

Wang X, Gordaninejad F (2006) Study of magnetorheological fluids at high shear rates. Rheol Acta 45:899–908. https://doi.org/10.1007/s00397-005-0058-y

Wereley NM, Chaudhuri A, Yoo J-H et al (2006) Bidisperse magnetorheological fluids using Fe particles at nanometer and micron scale. J Intell Mater Syst Struct 17:393–401. https://doi.org/10.1177/1045389X06056953

Zainordin AZ, Mohamed Z, Ahmad F (2021) Magnetorheological fluid: testing on automotive braking system. Int J Automot Mech Eng 18:8577–8584. https://doi.org/10.15282/ijame.18.1.2021.16.0651